CHEMISTRY
A EUROPEAN JOURNAL

DOI: 10.1002/chem.200700468

Thermodynamic Parameters Governing the Self-Assembly of Head–Head–Head Lanthanide Bimetallic Helicates

Thomas B. Jensen, Rosario Scopelliti, and Jean-Claude G. Bünzli*[a]

Abstract: The heterobitopic ligands L^{ABX} (X = 1, 2, 3, 4 or 5), differing only by a Cl or NEt_2 substituent, have been designed to complex with a pair of lanthanide ions to form triple-stranded bimetallic helicates of overall composition $[Ln_2(L^{ABX})_3]^{6+}$. The percentage of HHH (head–head–head) isomer, in which each of the three ligand strands coordinates to the same lanthanide ion with the same coordination unit, is deciding the ability of the ligands to selectively form heterobimetallic complexes containing one luminescent and one magnetic or two different luminescent ions. It deviates significantly from the statistical value of 25% and ranges from 6–20% for L^{AB2} complexes to 93–96% for L^{AB4} complexes. The equilibrium between HHT (head–head–tail) and HHH isomers has been investigated in detail for homobimetallic helicates (Ln = Y, La, Ce, Pr, Nd, Sm, Eu, Lu) by means of variable temperature NMR and thermodynamic parameters have been determined. The equilibrium is characterized by small values of ΔH and ΔS, which vary in opposite direction along the lanthanide series for complexes with the same ligand in a way that keeps the value of ΔG almost constant. The results are interpreted in terms of differences in interstrand stacking, ion–dipole interactions and metal–metal repulsion.

Keywords: bimetallic compounds · helical structures · lanthanides · thermodynamic parameters

Introduction

Lanthanide luminescent probes are presently the subject of a substantial interest in the field of biomedical analysis and imaging in view of the specific spectroscopic properties of trivalent lanthanide ions.[1–4] While development of time-resolved luminescent immunoassays is still a major target,[5–7] new highly luminescent lanthanide complexes are presently being tested for cell imaging and in cellulo determination of analytes.[8,9] Increasing the number of detectable probes on a single sample, for instance by designing stains with tunable emission wavelengths and simultaneously tunable excited-state lifetimes, is potentially interesting[10] and in this context, bimetallic functional edifices may therefore combine two luminescent or one magnetic and one luminescent centers in a single dual probe.

The insertion of a specific heteropair of lanthanide ions in a molecular framework is a difficult challenge in view of the limited differences in chemical properties and size of these ions.[1] Among several possible strategies leading to such an insertion,[11,12] we have chosen the self-assembly of triple-stranded heterometallic helicates in order to take advantage of the potential chirality of these edifices in future work.[12] Helicity is present in numerous chemical and biochemical systems, obvious examples being double-stranded DNA and triple-stranded collagen. While in the latter compounds the helicity is induced by hydrogen bonds, there are other means of producing such structures, for instance by conformational restriction or by coordination to metal ions resulting in self-assembled supramolecular helicates. A metal-containing helicate[13,14] results from specific interactions between the ligand strands and the metal ions. Its self-assembly can be tuned by the intrinsic properties of the metal ions: coordination number, stereochemical preferences, charge and electronic structure, kinetic stability, and affinity for the binding units grafted on the ligand strands. The advantage of inserting metal ions into helical structures lies in their spectroscopic and magnetic properties which can be either translated in the final helicates or even enhanced, because the regular arrangement of several metal ions along the same direction may result in unusual proper-

[a] Dr. T. B. Jensen, Dr. R. Scopelliti, Prof. Dr. J.-C. G. Bünzli
Laboratory of Lanthanide Supramolecular Chemistry
École Polytechnique Fédérale de Lausanne (EPFL)
LCSL-BCH 1401 Lausanne (Switzerland)
Fax: (+41) 21-693-9825
E-mail: jean-claude.bunzli@epfl.ch

Supporting information for this article is available on the WWW under http://www.chemeurj.org/ or from the author.

ties such as directional energy transfer or magnetic interactions.

Our laboratory has devoted much effort in building up a library of hexadentate ditopic ligands with bis(benzimidazole)pyridine cores. The initial symmetric ligand design, L^A (Scheme 1), tailored to induce nine-coordinate, tricapped

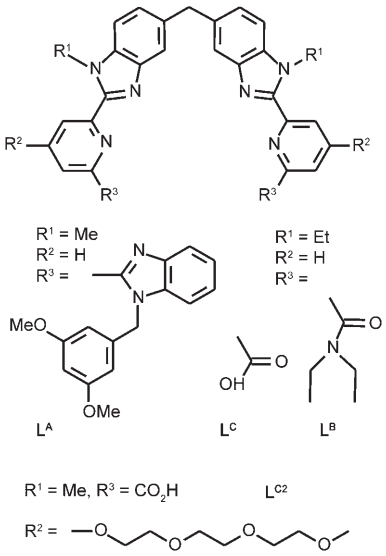

Scheme 1. Symmetrical ditopic ligands for self-assembling bimetallic lanthanide helicates.

trigonal prismatic environments around the 4f ions,[15] proved to be quite versatile: i) the terminal benzimidazole moieties can be replaced by amide (L^B)[16] or carboxylic acid (L^C)[17] functions, the latter allowing the helicates to form in water; ii) the 4-position of the pyridine rings can be substituted by Cl or Br[18] opening the way to the grafting of groups able to couple with biological material[19] or allowing the helicates with L^{C2} to diffuse into cells for imaging purposes.[20]

The heterobitopic ligand L^{AB1} (Scheme 2), combining the coordination units of L^A and L^B, was designed for incorporating two different lanthanide ions in the same helicate and it indeed forms self-assembled heterobimetallic helicates of composition $[Ln^1Ln^2(L^{AB1})_3]^{6+}$ in acetonitrile solution.[12]

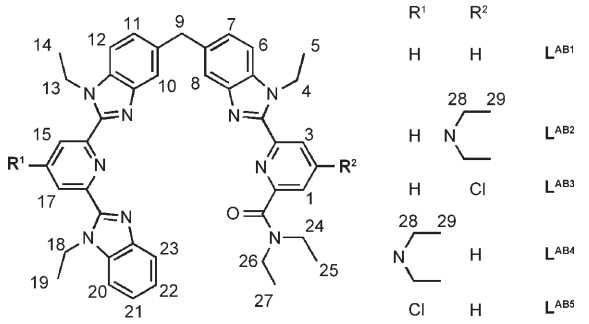

Scheme 2. Unsymmetrical ditopic hexadentate ligands studied herein with proton numbering used in the NMR spectra.

For the La/Lu couple the yield of hetero complexes exceeds 90% and this is closely related to the fact that L^{AB1} has a tendency to form high percentages of head–head–head (HHH) isomers (Figure 1). In the latter, all three ligand

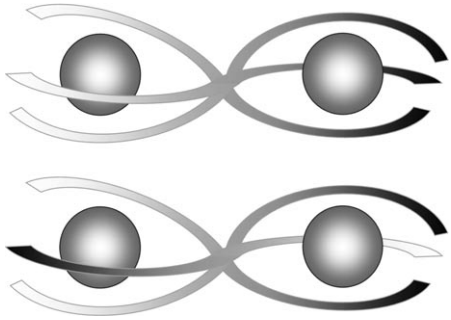

Figure 1. Schematic representation of the HHH (head–head–head; top) and HHT (head–head–tail; bottom) isomers of the $[Ln_2(L^{ABX})_3]^{6+}$ helicates.

strands are oriented in the same direction with carboxamide groups binding preferentially to smaller lanthanide ions. This behavior is further underlined by L^{AB2}, for which low HHH percentages of 6–20% result in low heterobimetallic yields.[21]

The thermodynamic parameters associated with the HHH selectivity have not yet received much attention, probably due to the inherent complexity of the systems and the small energy differences between the eight possible isomers for a heterobimetallic system. Recently, however, methods have been developed to extract the different contributions (ligand–metal, ligand–ligand and metal–metal) to the total free energy of triple stranded helicates containing two or more lanthanide ions.[22–24] To further our understanding of these contributions, we present here a detailed study of the thermodynamic parameters extracted from variable-temperature ^{1}H NMR spectra for homobimetallic $[Ln_2(L^{ABX})_3]^{6+}$ helicates with L^{AB1}, L^{AB2}, as well as with the related ligands L^{AB3}, L^{AB4} and L^{AB5} (Scheme 2, Ln = Y, La, Ce, Pr, Nd, Sm, Eu, and Lu). The crystal structure of the homobimetallic helicate $[Sm_2(L^{AB3})_3]^{6+}$ is also presented to enlighten the discussion.

Results and Discussion

Crystal and molecular structure of $[Sm_2(L^{AB3})_3](ClO_4)_6\cdot 5\,MeCN\cdot 2\,EtCN$: The compound is isostructural with the $[Ce_2(L^{AB3})_3](ClO_4)_6$ and $[NdLu(L^{AB3})_3](ClO_4)_6$ helicates[21] and crystallizes in the space group $P2_1/n$ with four formula units in the unit cell (Table S1, Figure S1, Supporting Information). The structure is made up of independent perchlorate anions, solvent molecules and complex cations of composition $[Sm_2(L^{AB3})_3]^{6+}$ (Figure 2) in which the three ligand strands are wrapped around the two nine-coordinate Sm^{III} ions in a helical fashion. The complex cations are pres-

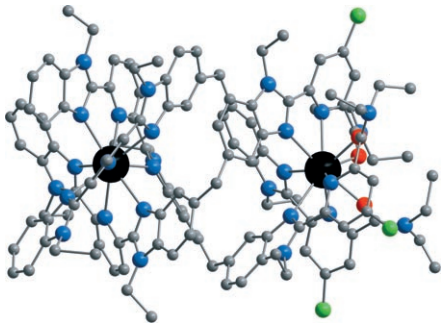

Figure 2. Representation of the molecular structure of the $[Sm_2(L^{AB3})_3]^{6+}$ cation (Sm atoms black, C atoms grey, N atoms blue, O atoms red, Cl atoms green).

ent as a racemic mixture of *P* and *M* isomers with the helix being either left- or right-handed. The configuration of the ligand strands is HHH, meaning that all three carboxamide oxygen atoms are coordinated to the same Sm^{III} ion.

The coordination geometry of the two Sm^{III} ions can be described as tricapped trigonal prismatic, where benzimidazole nitrogen atoms and carboxamide oxygen atoms form the prisms, which are capped by pyridine nitrogen atoms. The most significant deviation from a regular tricapped trigonal prism is that the upper and lower faces of the prisms are twisted by 12–13° with respect to each other. The mean Sm–N distance (Table 1) is 2.61(3) Å in both the

Table 1. Sm–N and Sm–O distances in the $[Sm_2(L^{AB3})_3]^{6+}$ ion.

Terminal benzimidazole		Pyridine		Bridging benzimidazole	
N1	2.598(9)	N3	2.60(1)	N4	2.621(9)
N10	2.612(9)	N12	2.632(9)	N13	2.585(9)
N19	2.65(1)	N21	2.579(9)	N22	2.592(8)
Bridging benzimidazole		**Pyridine**		**Carboxamide**	
N6	2.63(1)	N8	2.566(9)	O1	2.418(8)
N15	2.620(9)	N17	2.64(1)	O2	2.410(8)
N24	2.597(9)	N26	2.59(1)	O3	2.382(8)

SmN_9 and SmN_6O_3 arrangements while the average Sm–O distance amounts to 2.40(2) Å, leading to ionic radii of 1.15 and 1.13 Å, respectively, in good agreement with the reported value of 1.132 Å.[25] A complete analysis of the coordination polyhedra is given in the Supporting Information (Figure S2, S3; Table S2). The ligand arrangement is very similar to the ones reported for other complexes with ligands L^{AB1} and L^{AB3}, despite not all the compounds crystallizing in the same space group.

The Sm–Sm distance is 9.18(2) Å and the pitch (the distance for the helicate to make one complete turn) is 13.3(3) Å, both values being in the range of those found for other helicates with L^{AB1} and L^{AB3}.[21] The Sm^{III} helicate appears to be partly stabilized by very weak interstrand π–π interactions between aromatic groups. The shortest distance observed is 3.490(3) Å between the five-membered rings of two almost parallel imidazole groups (dihedral angle = 11.8(4)°, Figure S4; Supporting Information) belonging to the N_9 coordination cavity.

Thermodynamic parameters of the HHT/HHH equilibria: Equilibria (1) were examined in CD_3CN by means of ^1H NMR spectroscopy in the temperature range −40 to +50 °C.

$$HHT\text{-}[Ln_2(L^{ABX})_3]^{6+} \rightleftharpoons HHH\text{-}[Ln_2(L^{ABX})_3]^{6+} \quad K \qquad (1)$$

For the diamagnetic complexes (Ln = La, Y, Lu) the vicinity of protons H8 and H10 (Scheme 2) to aromatic benzimidazole groups on neighboring ligand strands results in their signals being shifted from the usual aromatic region to the less crowded 5.6–6.0 ppm range of the spectrum. In the HHH isomer all three ligand strands are equivalent and give rise to only one set of signals in the spectrum; in the HHT isomer each of the three non-equivalent ligand strands generates a set of signals (Figure 3). The relative concentrations

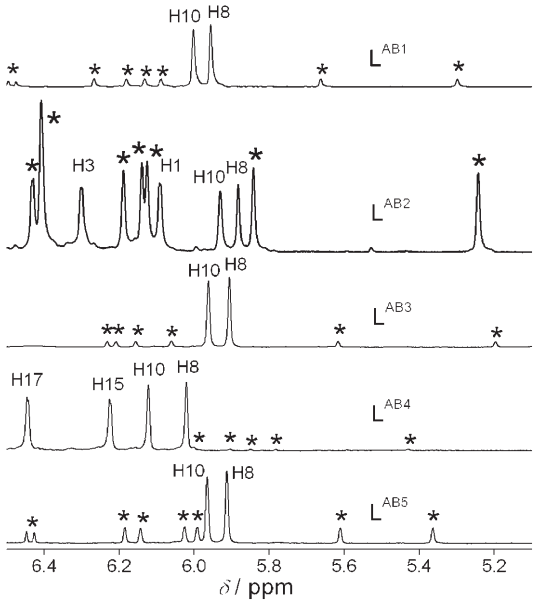

Figure 3. Partial ^1H NMR spectra of $[La_2(L^{ABX})_3]^{6+}$ complexes in CD_3CN solution. Assignments are for signals of the HHH isomer; HHT signals are denoted with stars.

of the two isomers can be directly calculated from the integrals of the respective signals. For the complexes with paramagnetic lanthanide ions (Ln = Ce, Pr, Nd, Sm, Eu) the H8 and H10 signals do not fall in this region and other signals have been chosen (see Figure 4 for an example). The influence of the temperature (−20 to +40 °C) on the NMR spectrum of $[La_2(L^{AB1})_3]^{6+}$ is illustrated in Figure 5.

The percentages of the HHH isomers at 25 °C and the resulting equilibrium constants *K* are listed in Tables S3–S7 (Supporting Information). Due to the high percentages of this isomer in the L^{AB4} complexes, integration of the HHT signals is difficult and lacks accuracy so that these com-

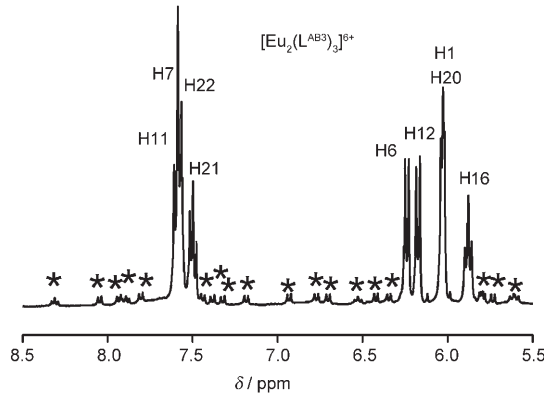

Figure 4. Partial ^{1}H NMR spectrum of $[Eu_2(L^{AB3})_3]^{6+}$. Assignments are for signals of the HHH isomer; HHT signals are denoted with stars.

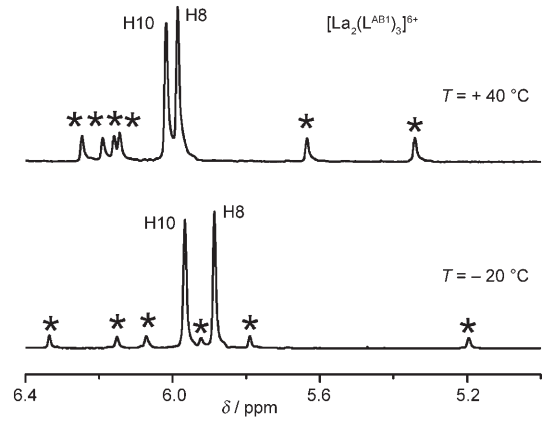

Figure 5. Partial ^{1}H NMR spectra of $[La_2(L^{AB1})_3]^{6+}$ showing the intensity variation as a function of temperature. Assignments are for signals of the HHH isomer; HHT signals are denoted with stars.

plexes have been left out of the subsequent data treatment. Values of ln$K$ were plotted against T^{-1} (Figure S5; Supporting Information) yielding straight lines with slopes $-\Delta H/R$ and intercepts $\Delta S/R$ from which values of ΔH, ΔS and ΔG could be calculated (Table 2).

For all complexes of a given ligand the values of ΔG are remarkably constant and do not depend, within experimental errors, upon the rare-earth ion (Table 2). This is, however, not the case for the enthalpic and entropic contributions (Figure 6). With two exceptions, $[Y(L^{AB1})_3]^{3+}$ and $[Lu(L^{AB1})_3]^{3+}$, the entropic contribution is unfavorable to the formation of the HHH isomers, as simple statistical considerations may suggest, while the enthalpic contribution is either favorable or close to zero.

For helicates with ligand L^{AB1}, the HHH isomer predominates and the unfavorable entropic contribution to ΔG decreases almost linearly along the lanthanide series, signifying that the HHH isomer is enthalpy-stabilized for the larger lanthanide ions, while it is entropy-stabilized for the smallest ions (Y, Lu).

When an electron-donating NEt_2 substituent is grafted in the 4-position of the pyridine group of the N_2O coordinating unit, the resulting helicates with L^{AB2} adopt preferentially the HHT configuration. At the beginning of the lanthanide series, the enthalpic contribution is favorable to the formation of the HHH isomer and is as large as for edifices with L^{AB1}, but it is overcome by a larger unfavorable entropic term. Enthalpy values increase up to Sm for which they reach essentially zero and then remain constant, so that the formation of the HHT isomers over the HHH species is entirely commanded by entropy. On the other hand, when the (weakly) electron attracting chlorine substituent is introduced in the same position, an entirely different situation emerges for L^{AB3}. The entropic contribution is around zero for La and then increases more or less linearly along the series; on the other hand, enthalpy decreases from -3 to -12 kJ mol^{-1} in going from La to Lu and is the driving force for the formation of the dominant HHH isomer all along the series.

Parameters influencing the HHH formation: As a starting point for the discussion, we consider a situation in which the ligand is symmetrical and the two metal ions have the same properties. The resulting hypothetical statistical mixture contains 25% HHH and 75% HHT isomers, yielding a constant of $^1/_3$ for Equilibrium (1). This corresponds to a ΔG^{stat} value

Table 2. Thermodynamic parameters for $[Ln_2(L^{ABX})_3]^{6+}$ complexes in CD_3CN with standard deviations between parentheses.

	La	Ce	Pr	Sm	Eu	Y	Lu
				L^{AB1}			
ΔH [kJ mol^{-1}]	−10.18(8)		−4.8(5)	−1.5(2)	−2.4(8)	−0.46(8)	1.9(2)
ΔS [J mol^{-1} K^{-1}]	−26.1(3)		−10(2)	0.1(7)	−1(3)	3.0(3)	12.6(8)
K (298 K)	2.6		2.0	1.8	2.2	1.7	2.1
% HHH (298 K)	73		67	65	69	63	68
				L^{AB2}			
ΔH [kJ mol^{-1}]	−10.7(4)	−2.9(5)	−4(1)	0.60(9)	1(1)	0.1(2)	1.1(4)
ΔS [J mol^{-1} K^{-1}]	−47(1)	−25(2)	−31(5)	−15.0(3)	−18(4)	−20.4(6)	−19(1)
K (298 K)	0.25	0.16	0.13	0.13	0.09	0.08	0.07
% HHH (298 K)	20	13	12	11	8	8	6
				L^{AB3}			
ΔH [kJ mol^{-1}]	−3.3(3)		−6.2(6)	−6.6(3)	−9.8(5)	−7.2(8)	−12(2)
ΔS [J mol^{-1} K^{-1}]	0(1)		−5(2)	−8(1)	−18(2)	−12(3)	−25(7)
K (298 K)	3.8		6.7	5.6	5.7	4.4	6.1
% HHH (298 K)	79		87	85	85	82	86
				L^{AB5}			
ΔH [kJ mol^{-1}]	−7.7(5)	−5.7(3)	−4.4(2)	−4.1(2)	−4.5(2)	−5.0(5)	−3.4(3)
ΔS [J mol^{-1} K^{-1}]	−23(2)	−18(1)	−13.8(8)	−11.8(6)	−13.9(8)	−13(2)	−8(1)
K (298 K)	1.5	1.1	1.1	1.2	1.2	1.6	1.5
% HHH (298 K)	60	53	53	56	54	61	60

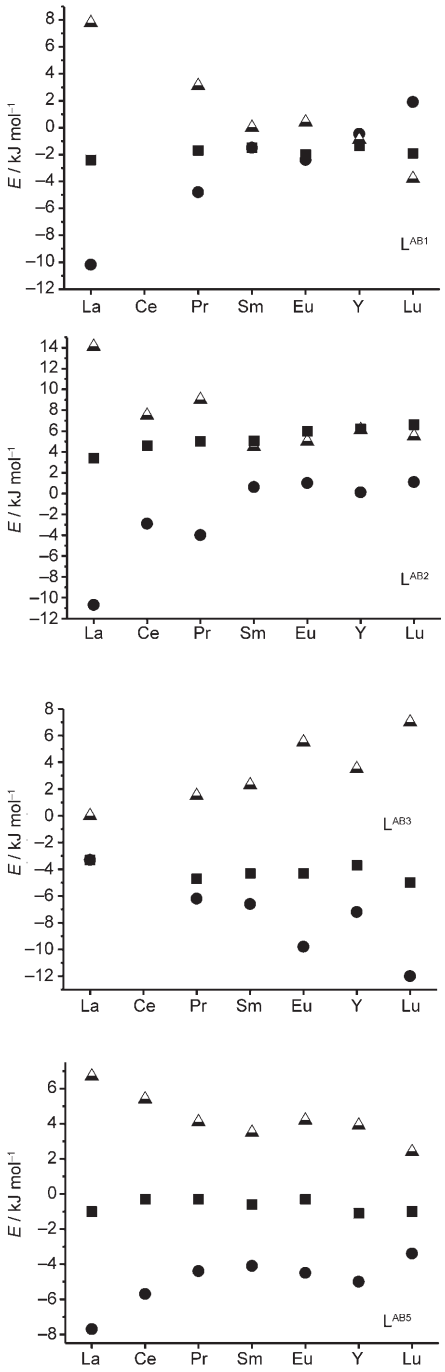

Figure 6. Graphical representation of the thermodynamic parameters for Equilibria (1); ●: ΔH, ▲: $-T\Delta S$, ■: ΔG.

of $+2.7\,\mathrm{kJ\,mol^{-1}}$. The assumption implies no enthalpy contribution so that only entropy ($-9.1\,\mathrm{J\,mol^{-1}\,K^{-1}}$ at 298 K) contributes to ΔG^{stat}. In Figure 7, on which the enthalpic contributions are plotted versus the entropic contributions, the corresponding values of ΔH^{stat}, $-T\Delta S^{stat}$, and ΔG^{stat} are indicated by dotted lines. The domain below and to the left of the ΔG^{stat} line indicates stabilization of the HHH isomer compared with the hypothetical statistical distribution. In addition, the ΔH^{stat} and $-T\Delta S^{stat}$ lines divide the figure in

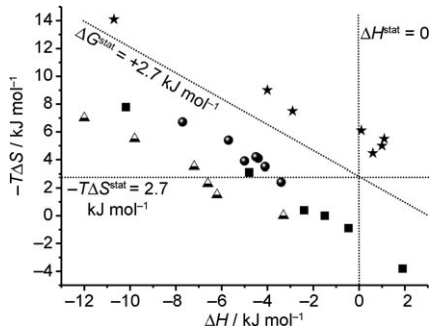

Figure 7. Entropic versus enthalpic contributions to the free energy of the HHT/HHH equilibria; ▲: L^{AB3}, ■: L^{AB1}, ●: L^{AB5}, ?starf;: L^{AB2}.

four quadrants. Values toward the bottom of the figure correspond to entropic stabilization of the HHH isomer; while values to the left indicate enthalpic stabilization.

Although ΔG values for Equilibria (1) are quite small, we try to rationalize them in terms of differences in the prevailing interactions in the helical edifices: i) the ion–dipole interactions between the coordination sites and the Ln ions, ii) the Ln–Ln Coulomb repulsion, iii) the organization energy required to build an hypothetical self-assembled helical receptor from the three ligand strands, and iv) interactions between the complex and the solvent. The 18 ion–dipole interactions are the strongest of the four contributions and relatively small differences in these interactions could lead to the observed energy differences between the HHH and HHT isomers. The Ln–Ln repulsion has been estimated to be on the order of $50\,\mathrm{kJ\,mol^{-1}}$ in the related helicates with L^B.[22] It depends on the Ln–Ln distance and the dielectric constant of the medium separating the two ions. While the former does not vary significantly upon changing the Ln ions,[12,21] the latter is expected to change with differences in the helical wrapping of the ligand strands. This wrapping is indeed the major difference in the structure of the helicates when the lanthanide ions are changed: as evidenced by the analysis of the coordination polyhedra in available crystal structures, the ligands are wrapped tighter around the smaller lanthanide ions.[12,21] It is, however, questionable whether these small structural differences can lead to variations of more than $10\,\mathrm{kJ\,mol^{-1}}$ along the lanthanide series. Also speaking against metal–metal repulsion being responsible for the effects observed here is the fact that the structural variation observed is the same for complexes of both L^{AB1} and L^{AB3}, whereas the variations in enthalpies found here are opposite for the two series of complexes.

The organization energy of the helical receptor includes interstrand interactions, in particular π-stacking interactions between aromatic groups on adjacent ligand strands. In the investigated complexes these interactions are very weak, with the shortest distances between such groups being around 3.5 Å, a value often taken as the highest limit for such interactions since it corresponds to the sum of the van der Waals radii. One of the aims of the present work was to test whether these interactions influence the position of

Equilibria (1) through substitution of the pyridine groups by electron-withdrawing substituents (e.g. Cl) which strengthen the interactions whereas electron-donating substituents (e.g. NEt_2) weaken them.[26,27] The solid-state structures of helicates with L^{AB1} and L^{AB3} are in line with the latter statement. In the reported crystal structures with L^{AB1}, the distances between the interacting planes are in the range 3.7–4.0 Å and the corresponding angles between 11.5 and 33.9°[12] while a stronger π-stacking interaction is seen in $[Sm_2(L^{AB3})_3]^{3+}$, see above. In the case of L^{AB1} helicates, we have demonstrated by lanthanide-induced NMR shifts that the solution structures closely match the single crystal structures[12] so that one may expect similar interstrand interactions in the two phases.

At first sight, the proportions of the HHH isomer obtained with L^{AB1} and L^{AB3} seem to substantiate the hypothesis of the influence of stabilizing weak π-stacking interactions at the N_9 end of the edifices, which do not exist for HHT isomers. A similar explanation has been given in the case of the prevalent facial versus meridional monometallic complexes with unsymmetrical aromatic tridentate N_2O ligands.[28] The chlorine substituent in L^{AB3} may favor π-stacking interactions at the N_6O_3 end of the helicate in addition to the larger π interaction at the N_9 end of the edifice found in the Sm helicate compared with L^{AB1} helicates. In line with this explanation are data for L^{AB2} since the diethylamine substituent which disfavors π-stacking interactions,[26,27] would then diminish the already very weak interstrand interactions at the N_6O_3 end of the helicate. However, data for L^{AB4} and L^{AB5} for which the substituents are bound to the N_3 coordinating unit which generates the π interaction are totally at variance with this explanation: the NEt_2 substituent now leads to >95% HHH isomers whereas the chlorine substituent diminishes the proportion of this isomer with respect to L^{AB1} helicates. Therefore, a first conclusion is that the π-stacking interstrand interactions are not always the main driven force in the predominance of one or the other isomer.

Since the stabilization of the HHH isomers, when it occurs, is entirely of enthalpic origin, except for $[Ln_2(L^{AB1})_3]^{3+}$ (Ln = Y, Lu) we have to turn to differences in ion–dipole interactions between the HHH (N_9/N_6O_3) and HHT (N_8O/N_7O_2) isomers.[1] The Ln–N distances observed in the reported structures[12] are independent of the coordination site, so that we do not expect noticeable differences in these interactions, but since they are large, minute variations may substantially contribute to the measured ΔG values. An interesting observation is the following. While the percentages of HHH isomers in homometallic systems with L^{AB1} lie in the range 63–73%, it increases substantially to 88% for the La–Ce heterobimetallic helicate and to ≈100% for all the other hetero pairs studied; for L^{AB3}, this percentage is ≈100%, whatever the heteropair considered.[21] This "additional" stabilization of the HHH species may be traced back to a better match of the N_9 cavity with larger Ln ions, as shown by the larger stability of the La helicate with L^A ($\log\beta_{23}$ = 20–22), compared with Lu ($\log\beta_{23}$ = 17)[15] and, also, by the stability trend of the monometallic helical tris complexes with bis(benzimidazole)pyridine with a drop in $\log K_3$ from 5.8 (La) to 2.7 (Lu).[29] On the other hand, the affinity of the N_2O coordinating sites of L^B for Ln ions only varies slightly along the series.[22] Since the chlorine substituent has a Hammett coefficient $\sigma = +0.23$,[30] it is not expected to induce a noticeable change in the electron density of the donor atoms of the tridentate coordinating units. As a consequence, its influence on the HHH proportion is not large, the latter increasing from (on average) 68% for L^{AB1} to 84% for L^{AB3} while it decreases to 57% for L^{AB5}. On the other hand, the electron donor substituent NEt_2 ($\sigma = -0.73$) modifies more the electron donating properties of the tridentate coordination units, resulting in a drop in the HHH percentage from 68% for L^{AB1} to 11% for L^{AB2} and to an increase to >95% for L^{AB4}.

Finally, this analysis does not consider solvent–helicate interactions but, although they are intrinsically large, we do not expect a great difference between the two isomers: experiments conducted in [D_6]acetone for the La and Lu helicates with L^{AB1} yielded very similar constants for Equilibria (1) compared with those in acetonitrile.[31]

Conclusion

The results presented here clearly illustrate how the self-assembly of metallosupramolecular lanthanide bimetallic helicates is governed by weak effects and interactions. In the investigated lanthanide-containing helicates, there is only 2–4 kJ mol^{-1} difference between the HHH and HHT isomers, while the selectivity of the former for a given hetero pair of lanthanide ions is much larger. Minute changes in the ligand design, for example, careful substitution of the pyridine 4-position of either tridentate N_3 or N_2O coordination units can drive the equilibrium towards an overall composition in solution dominated by only one of the two isomers. The data presented here prevent a quantitative analysis of the parameters prevailing to the formation of the HHH versus HHT isomer because too many such parameters are involved. On the other hand, they demonstrate that the effect is essentially enthalpy-driven and mainly governed by the electron-donating properties of the substituent while interstrand interactions seemingly play a less important role. This allows for qualitative predictions to be made as how to tune the formation of one isomer over the other and will therefore be most helpful in the directed self-assembly of new functional bimetallic helicates.

[1] Despite all our efforts, no single crystals of a HHT helicate could be isolated so far with any of the reported ligands.

Experimental Section

Preparation of ligands: L^{AB1},[12] L^{AB2} and L^{AB3}[21] were prepared according to published procedures. L^{AB4} and L^{AB5} were prepared using similar strategies;[31] the details will be published separately.

Preparation of complexes $[Ln_2(L^{ABX})_3](ClO_4)_6$: Partially dehydrated perchlorate salts $Ln(ClO_4)_3{\cdot}xH_2O$ (Ln = Y, La-Lu) were prepared from the corresponding oxides (Rhône-Poulenc, 99.99%) in the usual way.[32]

CAUTION! *Perchlorate salts combined with organic ligands are potentially explosive and should be handled in small quantities and with adequate precautions.*[33]

Stock solutions of $Ln(ClO_4)_3{\cdot}xH_2O$ in MeCN were obtained by weighting. The concentrations of the solutions were determined by complexometric titrations with $Na_2(H_2edta)$ in presence of urotropin using xylene orange as indicator.

NMR samples of $[Ln_2(L^{ABX})_3](ClO_4)_6$ complexes were prepared by reacting a weighed amount of L (3–15 mg) dissolved in CH_2Cl_2 with $^2/_3$ equivalents of $Ln(ClO_4)_3{\cdot}xH_20$ in the form of a MeCN solution. After stirring for 1–3 h the solution was evaporated to dryness, the residue was dried in vacuum at 50 °C and re-dissolved in 0.6 mL CD_3CN.

Spectroscopic measurements: MS spectra used for the characterization of organic compounds were recorded in MeOH or MeCN with a Finnigan SSQ-710C spectrometer. 1D ^{1}H NMR spectra were measured on a Bruker Avance 400 (400 MHz) spectrometer.

X-ray crystallography: X-ray quality crystals of $[Sm_2(L^{AB3})_3](ClO_4)_6{\cdot}5\,MeCN{\cdot}2\,EtCN$ were obtained by reacting $^2/_3$ equiv of $Sm(ClO_4)_3$ with 1 equiv L^{AB3} (10 mg) in MeCN solution. After evaporation to dryness and drying in vacuum the solid residue was re-dissolved in MeCN/EtCN 1:1 ($\approx$0.5 mL) and recrystallized by slow diffusion of *t*BuOMe at $T = -18$ °C. Data collection of a colorless crystal of $[Sm_2(L^{AB3})_3](ClO_4)_6{\cdot}5\,MeCN{\cdot}2\,EtCN$ has been performed at 140(2) K on an Oxford Diffraction Sapphire/KM4 CCD equipped with a kappa geometry goniometer. Data were then reduced using CrysAlis RED[34] and corrected for absorption by the DELABS algorithm.[35] Structure solution and refinement have been carried out by using SHELXTL.[36] The structure has been refined using the full-matrix-block least-squares on F^2. H atoms have been placed in calculated positions with the "riding" model. The solvent molecules have been retained as isotropic. Some restraints have been applied to solve the problems found in the last stages of refinement: a rigid bond restraint (DELU) has been applied to the entire structure whereas some geometric restraints (DFIX) have been applied to a disordered ClO_4^- and to some solvent molecules. The sample was a weak diffracting crystal which explains the relatively high R_1 factor.

CCDC-639865 contains the supplementary crystallographic data for this paper. These data can be obtained free of charge from The Cambridge Crystallographic Data Centre via www.ccdc.cam.ac.uk/data_request/cif.

Acknowledgement

This project is supported through grants from the Swiss National Science Foundation.

[1] J.-C. G. Bünzli, *Acc. Chem. Res.* **2006**, *39*, 53–61.
[2] J.-C. G. Bünzli, C. Piguet, *Chem. Soc. Rev.* **2005**, *34*, 1048–1077.
[3] S. Faulkner, S. J. A. Pope, B. P. Burton-Pye, *Appl. Spectrosc. Rev.* **2005**, *40*, 1–31.
[4] P. R. Selvin, *Annu. Rev. Biophys. Biomol. Struct.* **2002**, *31*, 275–302.
[5] S. Faulkner and J. L. Matthews, in *Comprehensive Coordination Chemistry II, Vol. 9* (Ed.: M. D. Ward), Elsevier Pergamon, Amsterdam, **2004**, Chapter 9.21, pp. 913–944.
[6] K. Matsumoto, J. G. Yuan *Lanthanide Chelates as Fluorescent Labels for Diagnostics and Biotechnology, Metal Ions in Biological Systems, Vol. 40* (Eds.: A. Sigel, H. Sigel), Marcel Dekker, New York, **2003**, Chapter 6.
[7] I. Hemmilä, V. M. Mukkala, *Crit. Rev. Clin. Lab. Sci.* **2001**, *38*, 441–519.
[8] S. Pandya, J. H. Yu, D. Parker, *Dalton Trans.* **2006**, 2757–2766.
[9] R. Pal, D. Parker, *Chem. Commun.* **2007**, 474–476.
[10] J. Y. Chen, P. R. Selvin, *J. Am. Chem. Soc.* **2000**, *122*, 657–660.
[11] J.-C. G. Bünzli, C. Piguet, *Chem. Rev.* **2002**, *102*, 1897–1928.
[12] N. André, T. B. Jensen, R. Scopelliti, D. Imbert, M. Elhabiri, G. Hopfgartner, C. Piguet, J.-C. G. Bünzli, *Inorg. Chem.* **2004**, *43*, 515–529, and references therein.
[13] J.-M. Lehn, A. Rigault, J. Siegel, J. M. Harrowfield, B. Chevrier, D. Moras, *Proc. Natl. Acad. Sci. USA* **1987**, *84*, 2565–2569.
[14] J.-M. Lehn, *Supramolecular Chemistry. Concepts and Perspectives*, VCH, Weinheim, **1995**.
[15] C. Piguet, J.-C. G. Bünzli, G. Bernardinelli, G. Hopfgartner, A. F. Williams, *J. Am. Chem. Soc.* **1993**, *115*, 8197–8206.
[16] N. Martin, J.-C. G. Bünzli, V. McKee, C. Piguet, G. Hopfgartner, *Inorg. Chem.* **1998**, *37*, 577–589.
[17] M. Elhabiri, R. Scopelliti, J.-C. G. Bünzli, C. Piguet, *J. Am. Chem. Soc.* **1999**, *121*, 10747–10762.
[18] C. Platas, M. Elhabiri, M. Hollenstein, J.-C. G. Bünzli, C. Piguet, *J. Chem. Soc. Dalton Trans.* **2000**, 2031–2043.
[19] R. Tripier, M. Hollenstein, M. Elhabiri, A.-S. Chauvin, G. Zucchi, C. Piguet, J.-C. G. Bünzli, *Helv. Chim. Acta* **2002**, *85*, 1915–1929.
[20] C. Vandevyver, A.-S. Chauvin, S. Comby, J.-C. G. Bünzli, *Chem. Commun.* **2007**, 1716–1718.
[21] T. B. Jensen, R. Scopelliti, J.-C. G. Bünzli, *Inorg. Chem.* **2006**, *45*, 7806–7814.
[22] K. Zeckert, J. Hamacek, J. P. Rivera, S. Floquet, A. Pinto, M. Borkovec, C. Piguet, *J. Am. Chem. Soc.* **2004**, *126*, 11589–11601.
[23] C. Piguet, M. Borkovec, J. Hamacek, K. Zeckert, *Coord. Chem. Rev.* **2005**, *249*, 705–729.
[24] J. Hamacek, M. Borkovec, C. Piguet, *Dalton Trans.* **2006**, 1473–1490.
[25] R. D. Shannon, *Acta Crystallogr. Sect. A* **1976**, *32*, 751–767.
[26] F. Cozzi, M. Cinquini, R. Annunziata, T. Dwyer, J. S. Siegel, *J. Am. Chem. Soc.* **1992**, *114*, 5729–5733.
[27] F. Cozzi, M. Cinquini, R. Annuziata, J. S. Siegel, *J. Am. Chem. Soc.* **1993**, *115*, 5330–5331.
[28] T. Le Borgne, P. Altmann, N. André, J.-C. G. Bünzli, G. Bernardinelli, P.-Y. Morgantini, J. Weber, C. Piguet, *J. Chem. Soc. Dalton Trans.* **2004**, 723–733.
[29] S. Petoud, J.-C. G. Bünzli, F. Renaud, C. Piguet, K. J. Schenk, G. Hopfgartner, *Inorg. Chem.* **1997**, *36*, 5750–5760.
[30] C. Hansch, A. Leo, R. W. Taft, *Chem. Rev.* **1991**, *91*, 165–195.
[31] T. B. Jensen, PhD Dissertation Nr. 3519, École Polytechnique Fédérale, Lausanne (EPFL), **2006**.
[32] J. F. Desreux, in *Lanthanide Probes in Life, Chemical and Earth Sciences. Theory and Practice* (Eds.: J.-C. G. Bünzli, G. R. Choppin), Elsevier, Amsterdam, **1989**, Chapter 2, pp. 43–64.
[33] W. C. Wolsey, *J. Chem. Educ.* **1973**, *50*, A335–A337.
[34] CrysAlis RED version 1.7.0, Oxford Diffraction Ltd., Abingdon, OX14 4RX, Oxfordshire (UK), **2003**.
[35] N. Walker, D. Stuart, *Acta Crystallogr. Sect. A* **1983**, *39*, 158–166.
[36] G. M. Sheldrick, *Acta Crystallogr. Sect. A* **1997**, *46*, 467–473.

Received: March 26, 2007
Published online: June 28, 2007

